Pergamon

Atmospheric Environment Vol. 32, No. 6, pp. 967–982, 1998

1352–2310/98 $19.00 + 0.00

PII: S1352–2310(97)00129–5

ORIGIN AND GROWTH OF WEATHERING CRUSTS ON ANCIENT MARBLES IN INDUSTRIAL ATMOSPHERE

A. MOROPOULOU,* K. BISBIKOU,* K. TORFS,† R. VAN GRIEKEN,† F. ZEZZA‡ and F. MACRI‡

*Department of Chemical Engineering, Material Science and Engineering Sector, National Technical University of Athens, Zografou Campus, 9 Iroon Polytechniou Street, Zografou 157 80,Athens, Greece; †Department of Chemistry, University of Antwerp (U.I.A.), Universiteitsplein 1, B-2610 Antwerp, Belgium; and ‡Istituto di Geologia Applicata e Geotecnica, Facolta di Ingegneria, Politecnico di Bari, Via Re David 200, I-70125 Bari, Italy.

(*First received* 27 *June* 1995 *and in final form* 1 *March* 1997. *Published March* 1998)

Abstract—The origin and growth of weathering crusts on the ancient marbles of ruins of the Sanctuary of Demeter in the industrial atmosphere of Eleusis in Greece have been investigated. A systematic mineralogical, petrographical and chemical examination of weathered stones and crusts was performed, both *in situ* and in the lab, on samples taken from different parts of the monument in relation to the surface characteristics as well as to the exposure to rain, sea-salt spray and wet and dry deposition of airborne pollutants and dust. In particular, the various material–environment interactions take place, are characterized by (a) disintegrated "washed-out" surfaces, where products are taken away through dissolution, (b) rusty yellow patinas rich in Fe and Cu, (c) firmly attached black crusts in contact with percolating water, where recrystallized calcite shields amorphous deposits rich in S, Si, Fe and carbonaceous particles, (d) black loose deposits in the water sheltered areas, consisting mainly of gypsum and fly ash particles and (e) cementitious crusts, coating and pitting the horizontal surfaces. Moreover, an interconnected evolution of various physicochemical processes is shown, characteristic of the origin and growth of various crusts, which are formed and classified accordingly.

Key word index: Patinas, cementitious encrustations, black crusts, air pollution, marble weathering, environment–material interactions.

INTRODUCTION

The degree and the distribution of the main types of observable rock deterioration in an urban environment are related to different kinds of wetting and particularly to the exposure of the stone surface to rain (Camuffo *et al*., 1983). In a polluted environment, two kinds of crusts are usually developed on calcareous rocks; the so-called "white" and "black" crusts.

White crusts are formed through the dissolution of gypsum and the reprecipitation of calcite at the surfaces that are subjected to wash out (Camuffo *et al*., 1987), which takes away the deposits and the products of dissolution (Camuffo *et al*., 1982). On the other hand, black crusts are developed by gypsum formation on surfaces sheltered from water and attacked by an SO_2-polluted atmosphere. On those areas protected from intensive wash-out, SO_2 and water vapour or rain water diffuse at a high rate through the pores towards the $CaCO_3$–gypsum interface. Thus, new porous gypsum film layers must be formed at the $CaCO_3$–gypsum interface. As the thickness of the gypsum increases, the number and length of the pores decrease due to the larger molecular volume of gypsum compared with that of $CaCO_3$ and finally, at ca. 30 nm thickness of gypsum, the pores cease to exist. Thereafter, the rate-determining step becomes solid-state diffusion of Ca^{2+} towards the environment (Skoulikidis and Charalambous, 1981). The transformation of the stone into gypsum is not only associated with the presence of gaseous SO_2, but also with S contained in the residual carbonaceous particles of combustion of fossil fuels for domestic heating (Del Monte *et al*., 1984). A high uptake of atmospheric particulate matter (Fe_2O_3, Al_2O_3, SiO_2, C, etc.) is observed on the weathered surfaces (Moropoulou and Bisbikou, 1995; Rodriguez-Navarro and Sebastian, 1995; Sabbioni, 1995). Silicate particles are emitted by, e.g. the combustion of coal and they are deposited at the exposed surfaces (Camuffo *et al*., 1987). Various intermediate crust formations are referred to in the literature, according to the wetting type of the surface. However, a number of physicochemical processes

determining the origin and growth of deteriorating crusts should be studied with respect to the type of the environmental attack (industrial and marine atmosphere, various types of total suspended particles, etc.) and the type of the respective surface.

The variation of climatic conditions (temperature, air humidity, etc.) contribute substantially to the creation of salts within the pores (Theoulakis and Moropoulou, 1988). NaCl gives rise to the gypsum solubility. The ratio of SO_4^{2-}/Cl^- in rain water varies according to the amounts of SO_2 in the atmosphere and characterizes the pollution level.

The micro-structural characteristics of the various lithotypes could act as criteria to evaluate their susceptibility to the weathering phenomena caused by the different environmental factors acting. Stones with large pores like marble may contain large amounts of water; stones with very small pores, although they may contain minor amounts of water, experience more frequently condensation and water may remain longer in the pores. The microstructure is also determining the mechanical weathering which accompanies the formation of the crusts on the stone surfaces, due to the polluted atmosphere.

In the present work, the marbles of the ruins of the Demeter Sanctuary in Eleusis, Greece, were subjected to detailed investigation.

The first temple of Demeter and the Eleusinian Sanctuary were founded in the reign of the legendary King Celeus in the Late Helladic period (1500–1425 BC), as a home for Demeter. The present ruins of the Telestirion (Fig. 1) belong to its fourth last building phase design by Ictinus in the Periclean period (Preka-Alexandri, 1991).

The Greater Eleusis area had been a rural area for years, but in the post-war period has become increasingly industrialized, with key manufacturing sectors, basically metallurgical and chemical ones. The Thriasian plain, in particular, has been dramatically "attacked" by several large and small industries causing a decline in environmental standards. In addition, the air pollutants, swept by the prevailing winds to the sea side, remain in Saronikos Bay for a period of time and then recirculate at the coastal areas increasing pollution problems. Air pollution creates aggressive atmospheric conditions which can damage the material cultural heritage of a region. Consequently, the Eleusis area corresponds to a typical urban-centre profile of intense and diversified industrial activity characterized by a highly polluted atmosphere heavily charged by suspended particles (Abazoglou *et al.*, 1990a, b). Hence, the study of neoformations on the monument surfaces in the archaeological site of Eleusis illustrates the variety of stone decay phenomena caused by air pollution and specifically by suspended particle attack, most probably in synergy with marine spray, due to the vicinity to the sea (Zezza, 1994).

Five different carbonate rocks (grey-micritic limestone, white Pentelic marble, white–grey marble, yellow limestone and biomicritic grey limestone) have been identified as building materials in the Sanctuary

Fig. 1. General view of the Demeter Sanctuary in Eleusis.

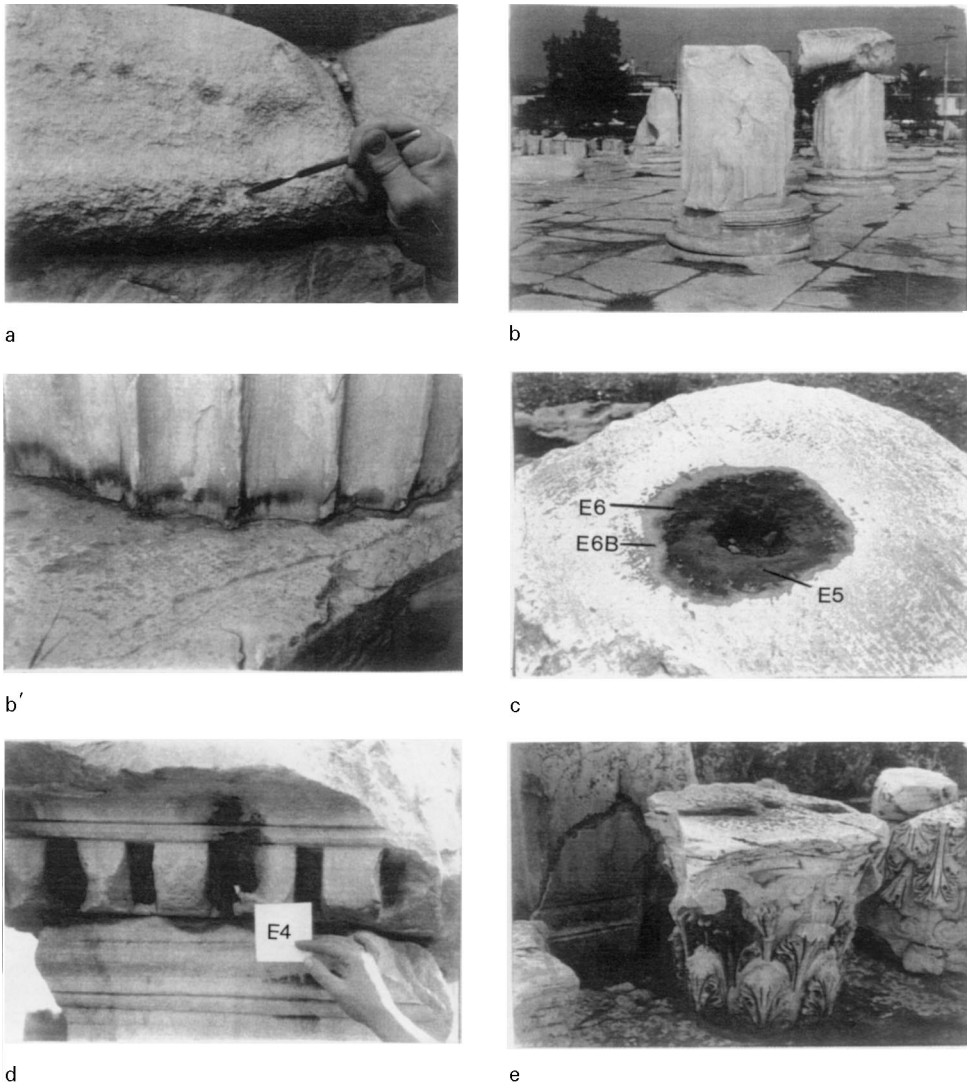

Fig. 2. Main decay patterns. Detachment (granular disintegration) along with rusty-yellow crusts (sample B1) (a). Rusty-yellow crusts at washed-out surfaces and where water-rebound phenomena occur (b-b′) (b′ = sample A2). Pitting on marble surfaces covered by cementitious encrustations (sample E5) and at the other edge, a grey–yellow crust (sample E6) is formed continuing at a washed-out surface (sample E6B) (c). Black crust in the form of loose deposits (sample E4) (d). Black–grey crust firmly attached to the surface (e).

(Moropoulou *et al*., 1994a, b); the scope of this work is mainly limited to the weathering of Pentelic marble.

Calcite comprises 96% of Pentelic marble, with about 1.8% dolomite. The remainder of the stone consists of minor quartz and fine silicate minerals (0.79% SiO_2, 0.52% Al_2O_3 and 0.12% FeO) (Dickinson *et al*., 1988). The petrographic analysis (Moropoulou *et al*., 1995) shows a medium-grained well recrystallized marble with granoblastic polygonal texture. The grain size indicates increasing intensity of metamorphism that is possibly attributed to high temperature and low deformation rates. The microstructural analysis (Moropoulou *et al*., 1995) shows a low total porosity (3.64 vol%) of interparticles type, characterized by a network of large fracturing pores between grains. High apparent density (2.71 $g\,cm^{-3}$), low water absorption (0.22%), as well as the wave velocity (5830 $m\,s^{-1}$) depending on the homogeneity of the stone mass, characterize the Pentelic marble.

The main decay patterns in the sequence of decreasing frequency with which they are observed, can be classified as follows:

— granular disintegration and detachment (Fig. 2a), the most general and important weathering on yellowish limestone and marble, presented at washed-out surface areas, or at surface areas facing the sea,
— crusts indicating biological attack to the stone,

Table 1. Description of the samples

Sample	Type	Location
E1	Black-grey crust on the white marble	Triumphal Arch, front side exposed to northern winds
E2	Washed-out surface, white-yellowish crust on the marble	Triumphal Arch, left side exposed to eastern winds
E3	Washed-out on the white marble	Triumphal Arch, back side exposed to southern winds
E4	Black crust on the white marble (loose deposit)	Triumphal Arch, right back side exposed to southern winds
E5	Cementitious crust, pit on the white marble	Column on the right side of the Triumphal Arch, exposed to all wind directions
E6	Yellow-grey crust at the edge of the pit	Column on the right side of the Triumphal Arch
E6B	Washed-out area on the marble as a continue of E6	
E7	Dust gathered on the marble horizontal surface	Triumphal Arch, shelter of a dentil, front side exposed to northern winds
E8	Column sample of accumulated dust and particle deposits in depth	Hole of a column on the right side of the Lesser Propylea, exposed to all wind directions
E9	Cementitious crust on a limestone surface	Wall on the left side of the Lesser Propylea, exposed to all wind directions
A1	Rusty-yellow crust on the white marble	Great Propylea, lying column
A2	Grey–rusty-yellow crust on the white marble	Great Propylea at the base of the column and especially where water rebound phenomena occur
B1	Disintegrated marble facing the sea	Wall at the south gate of Holy Place

— chromatic alteration from the white of the Pentelic marble to the rusty-yellow colour at the washed-out surfaces (Fig. 2b) and mainly where water-rebound phenomena occur (Fig. 2b′),
— pitting on the marble and limestone surfaces covered by cementitious encrustations, especially on the horizontal surfaces like pavements (Fig. 2c),
— black crust formations in the form of loose deposits, formed at the surfaces sheltered from rain water and presenting an anomalous relief with high friability (Fig. 2d),
— black–grey thin crust formations, firmly attached underneath cornices and pillar crowns as well as on the exposed upper perpendicular surfaces, wherever the marble surfaces are in contact with percolating rain water but are not washed out (Fig. 2e).

The real weathering phenomena are usually a combination of the above simplified forms used for the convenience of the analytical study.

In the present work, systematic mineralogical, petrographical and chemical examination is performed on samples from the Eleusis Sanctuary ruins, in an effort to interpret the deterioration phenomena that take place.

MATERIALS AND METHODS

Thirteen samples of crusts, dust deposits and encrustations, are presented in Table 1, taken from different parts of the monument, as it was proved from the preliminary examinations, according to:

— the decay pattern and the damage levels, assessed through macroscopic observation,
— the orientation of the individual architectural elements,
— the degree of sheltering from rain water (black areas),
— the exposure to direct rainfall (washed-out areas).

Experimental procedure

Chemical analyses and microanalyses have been performed on the crust samples by using ion chromatography (IC), atomic absorption and atomic emission spectrometry (AAS and AES), energy dispersive X-ray fluorescence (EDXRF), electron probe micro-analysis (EPMA) and Fourier transform laser microprobe mass spectrometry (FT-LMMS). The mineralogy, fabrication and texture of the crusts were studied by scanning electron microscopy with energy dispersion X-ray analysis (SEM-EDX) and X-ray diffraction analysis (XRD), in order to extract conclusions on the environment-materials interactions taking place on the monument surfaces and in depth.

Electron probe micro-analysis (EPMA) and scanning electron microscopy—energy-dispersive X-ray analysis (SEM-EDX). The samples were carbon-coated in order to make them conductive. To analyse the sample composition in depth, the sample was embedded in a resin. The sample was cut perpendicularly to the weathered crust, and polished without water.

The instrument used for EPMA was a JEOL JXA-733 Superprobe, equipped with a Tracor Northern TN 2000 energy-dispersive X-ray detector. For scanning electron microscopy, a JEOL-JSM 6300 scanning microscope was used. The samples were excited by an electron beam of 1 nA and an electron energy of 25 keV for EPMA, and 15 keV for SEM.

By recording energy-dispersive X-ray spectra of subsequent small areas, perpendicular to the exposed surface, depth profiles were obtained, showing the elemental distribution through the sample, when proceeding from the outer surface layer towards the unaffected inner part. The concentrations of the elements are expressed in weight percent. They were calculated after ZAF-correction, using a quantitative program. Only the major elements from the EDX-analysis are presented in the depth profiles. The depth profiles, measured with EPMA, and the micrographs of weathered layers and deposited particles, together with the

Table 2a. Results of IC, AAS and AES (concentrations are expressed in weight percent of the dissolved sample)

Sample	Cl^-	NO_3^-	SO_4^{2-}	Ca^{2+}	Mg^{2+}	Na^+	K^+
E1	0.13	0.00	39.4	20.4	0.04	0.11	0.03
E3	0.33	0.00	0.11	4.24	0.03	0.02	0.00
E4	0.29	0.24	57.2	22.8	0.06	0.16	0.09
E5	0.25	0.19	47.8	23.4	0.05	0.22	0.04
E6	0.16	0.39	10.9	6.45	0.05	0.15	0.19
E6B	0.18	0.21	4.51	5.12	0.08	0.27	0.10
E7	0.76	0.00	45.3	23.9	0.04	0.12	0.02
E8	0.90	0.56	2.43	17.9	0.37	1.49	1.29
E9	0.54	1.36	60.8	21.5	0.01	8.29	2.38
B1	0.21	0.02	20.7	15.9	0.11	0.42	0.34

Table 2b. Correlation matrix, as calculated from the IC, AAS and AES results

	Cl^-	NO_3^-	SO_4^{2-}	Ca^{2+}	Mg^{2+}	Na^+	K^+
Cl^-	1.00						
NO_3^-	0.34	1.00					
SO_4^{2-}	0.03	0.30	1.00				
Ca^{2+}	0.37	0.17	0.83	1.00			
Mg^{2+}	0.57	0.09	− 0.47	0.02	1.00		
Na^+	0.32	0.93	0.41	0.25	− 0.09	1.00	
K^+	0.50	0.94	0.22	0.24	0.26	0.94	1.00

corresponding X-ray spectra, obtained by SEM-EDX, are presented in Fig. 3–7.

Ion chromatography (*IC*), *atomic absorption spectrometry* (*AAS*) *and atomic emission spectrometry* (*AES*). The samples were crushed in an agate mortar and about 100 mg of the resulting powder was dispersed in 100 ml distilled water. The aqueous suspension was filtered through a Millipore 0.2 μm pore-size filter and the filtrate was analysed. The anions (Cl^-, NO_3^- and SO_4^{2-}) in the filtrate were determined by a Dionex 4000i Ion Chromatograph, equipped with a AS11 separator column; the eluent was 20 mM NaOH. The cations Ca^{2+} and Mg^{2+} were determined by means of atomic absorption spectroscopy (AAS), whereas Na^+ and K^+ were measured by atomic emission spectroscopy (AES), both by means of a Perkin–Elmer 3030 spectrometer. The samples were acidified to pH 2 by using HCl, and a 10% La^{3+} solution was added to the samples to avoid interferences. The average of 3 measurements was used. The concentrations of the ions in the stones are expressed in weight percent to the dissolved mass of the stone sample. Table 2 shows the IC, AAS and AES results for the soluble crust samples.

Energy-dispersive X-ray fluorescence analysis (*EDXRF*). About 1 g of the crust samples was wet-ground for about one minute in a McCrone Micronizing Mill. A few millilitres of the suspension was brought on a Mylar foil, which was glued on a Teflon ring, to obtain a sample thickness of around 1 mg cm^{-2}. The foil was dried in an oven at a temperature of 60°C. Analyses were carried out using a Tracor Spectrace 5000 instrument. The instrument was equipped with a Si(Li) detector and a low power X-ray tube with a Rh target, controlled by an IBM computer. The X-ray spectra were accumulated during 3000 s and analysed using the AXIL software (Van Espen *et al*., 1986). Soil standards: IAEA Soil 5 and BCR 142 were used to check the accuracy of the measurements. Table 3 shows the EDXRF results.

X-ray diffraction analysis (*XRD*). XRD analysis was performed, using a Siemens D-500 X-ray Diffractometer, based on an automatic adjustment and analysis system with a Diffract-EVA qualitative analysis software, in order to check whether crystalline phases may be interrelated with possible transformations between dust and suspended particle deposits as well as with surface encrustations (cementitious crusts). The results are presented in the Table 4.

Fourier transform—laser microprobe mass spectrometry (*FT-LMMS*). LMMS employs focused laser-beam irradiation of solids and subsequent mass analysis of the ions produced. The technique is suitable for the local analysis of inorganic and organic constituents with a spatial resolution in the micrometer range. The Fourier transform (FT) ion cyclotron resonance mass spectrometer is an analyser of choice for LMMS because high mass resolution and accurate mass determination can be routinely achieved at adequate sensitivity (Van Vaeck *et al*., 1993). The FT-LMMS instrument development was based on a Spectrospin CMS 47X MicroFocus instrument (Spectrospin, Fällanden, Switzerland). Some results from the cement encrustation of sample E9 are included in Fig. 7.

RESULTS AND DISCUSSION

Table 2 presents the results of IC, AAS and AES on the leachate samples. It can be seen that some of the leachates contain a large quantity of SO_4^{2-}, in particular, in the black crust sample (E4: 57%), in the black–grey crust (sample E1: 40%), in the cementitious crust (sample E9: 60% and sample E5: 48%) and ca. 45% in the dust from the water-shielded surface of a dentil (sample E7), which has the same composition as sample E1 from that side. In the dust column sample (sample E8), from the crown pillar in contact with water, most salts have already been washed

Table 3. Results of EDXRF (concentrations are expressed in % or ppm, as indicated in the table)

	A1	A2	E1	E3	E4	E5	E6	E7	E8	E9	B1
Si (%)	2.96	5.20	3.50	0.93	2.60	3.80	1.90	16.8	N.M.	N.M.	N.M.
P (ppm)	N.D.	N.D.	N.D.	N.D.	N.D.	N.D.	N.D.	1.90	N.M.	N.M.	N.M.
S (%)	0.14	0.42	2.60	0.13	1.90	0.25	0.14	20.8	N.M.	N.M.	N.M.
Cl (%)	0.27	0.43	0.33	N.D.	0.51	N.D.	N.D.	0.46	N.M.	N.M.	N.M.
K (ppm)	1.22%	1.08%	6540	7790	6430	7490	7510	6190	1.06%	4550	2260
Ca (%)	37.3	33.7	29.2	38.7	31.0	32.8	36.3	14.6	20.5	23.7	43.2
Ti (ppm)	87.9	N.D.	281	75.8	192	302	242	1010	1910	837	181
V (ppm)	N.D.	N.D.	N.D.	N.D.	N.D.	N.D.	N.D.	58.5	N.D.	N.D.	N.D.
Cr (ppm)	35.9	N.D.	61.2	N.D.	40.3	N.D.	32.1	96.7	194	105	N.D.
Mn (ppm)	186	197	323	195	148	385	360	229	559	397	N.D.
Fe (ppm)	934	1170	4000	625	2540	4070	2370	1.36%	2.63%	1.87%	501
Ni (ppm)	N.D.	N.D.	11.0	N.D.	15.9	20.2	8.48	56.9	108	47.7	N.D.
Cu (ppm)	N.D.	17.4	35.3	N.D.	39.4	23.5	9.66	58.9	111	47.7	7.09
Zn (ppm)	48.1	59.0	94.6	19.8	77.0	136	56.7	238	499	226	37.5
Ga (ppm)	N.D.	N.D.	N.D.	N.D.	N.D.	N.D.	N.D.	6.47	10.0	10.0	2.68
Ge (ppm)	N.D.	9.97	5.37	9.43	6.50	6.38	7.33	N.D.	N.D.	N.D.	N.D.
As (ppm)	N.D.	N.D.	N.D.	N.D.	N.D.	N.D.	N.D.	N.D.	51.7	20.0	N.D.
Br (ppm)	N.D.	N.D.	5.29	N.D.	12.6	4.71	N.D.	7.95	9.53	5.93	N.D.
Rb (ppm)	7.15	N.D.	15.9	6.90	11.3	20.3	10.2	34.4	37.1	23.9	3.74
Sr (ppm)	220	230	216	177	203	204	194	177	346	250	148
Y (ppm)	13.7	16.3	14.7	14.4	7.68	11.9	13.0	12.0	18.2	10.6	11.0
Zr (ppm)	20.4	53.3	45.5	7.60	28.3	18.5	11.0	57.3	106	70.3	18.2
Ba (ppm)	N.D.	N.D.	N.D.	N.D.	N.D.	546	N.D.	545	N.D.	738	N.D.
Pb (ppm)	101	N.D.	89.6	N.D.	85.5	270	119	304	354	322	23.4

Note: N.D., not determinable, i.e. below the detection limit; N.M., not measured.

Table 4. XRD Results

Sample	Calcite	Quartz	Gypsum	Dolomite	Alkali-feldspars-plagioclase	Mica	Chlorite	Calcium Silicate Hydrate (CSH)	Halite
E1	+ +	+	+	−	+ +	+ +	−	−	+
	+ +	+	+						
E2	+ +	+	+	−	+ +	+ +	−	−	−
E4	+ +	+ +	+ +	−	−	−	−	−	−
	+		+						
E6	+ +	+ +	+ +	−	+ +	+ +	−	−	+
	+	+							
E7		+	+	+	+ +	+ +	+	−	−
		+		+					
E8	+ +	+	−	+ +	+ +	+ +	−	+	−
	+ +	+	+	+					
E9	+ +	+	+	−	+ +	+ +	+	+	−

Note: + + + +, very abundant; + + +, abundant; + +, present; +, small amount.

away. The washed-out samples (E3 and E6B) contain low quantities of sulphate. The low K^+, Na^+ and Cl^- contents may, most probably, be attributed to the detachment of marble granules along with salt crystals, seen in other cases of marine spray corrosion (Moropoulou *et al*., 1994a, b), as well.

The relationship between the ions in the leachate samples is considered by use of the correlation coefficient. This coefficient may be viewed as providing a measure of the mutuality of the relationship between two variables, notwithstanding they influence each other or are influenced by any other variables. The correlation coefficient reaches 1 if the variables are correlated. The correlation matrix of the concentrations of the ions is presented in Table 2b. Ca^{2+} and SO_4^{2-} are highly correlated. Na^+, K^+ and NO_3^- are interrelated. Cl^- is only slightly related to the Mg^{2+} content. Only 1/3 of Cl^- originates from marine spray, while 2/3 originates from anthropogenic provenance.

From the EDXRF results (Table 3), it is clear that all samples contain much Si, Ca, S, Fe, Cl and K. It could be supposed that most of the Si and Fe is due to the cement production in the neighbourhood of the temple. The samples from the Great Propylea (A1, A2) contain a large amount of Si, but lower Fe concentrations than the crust samples E1 and E4. In the sample from the wall facing the sea (B1), almost only Ca has been found. The black crusts (E1 and E4) are enriched in Ca, S, Si, Fe and K. The high concentration of S can be explained as gypsum. The dust from the front (E7) contains almost pure gypsum (20% S and 15% Ca); Fe (1%) and Si (16%) are present as well; more Ti, possibly due to the cement industry, has been found in this sample in comparison with the other samples as well as Cl, most probably due to marine spray. The dust sample E8, as well as the cementitious crust (sample E9), are enriched in Fe, Ti (due to industry) and Pb. The washed-out sample from the pit (E6) contains much Ca and Fe.

It might be assumed that the analytical results of IC, AAS, AES and EDXRF alone are not sufficient to classify and interpret the crust growth mechanisms. However, they do provide some valuable information about the origin of the crusts, which have to be further correlated quantitatively.

The XRD results (Table 4) provide more information on the crystalline components. The black–grey crust (E1) contains calcite, quartz, gypsum and halite (Table 2). The loose deposits (E4) consist almost entirely of gypsum. The washed-out E2 sample is composed exclusively of calcite, quartz, feldspars, gypsum and mica, while E6 is differentiated by the presence of halite. The cementitious crust (E9) presents cementitious CSH phases (i.e. calcium silicate hydrates, C = calcium-oxide, S = silicate, H = water, e.g. $3CaO \cdot 2SiO_2 \cdot 3H_2O$). The dust deposits are differentiated. Gypsum is present in E7, and cementitious CSH phases in E8. Moreover, E7 contains more dolomite than calcite which is mainly present in E8.

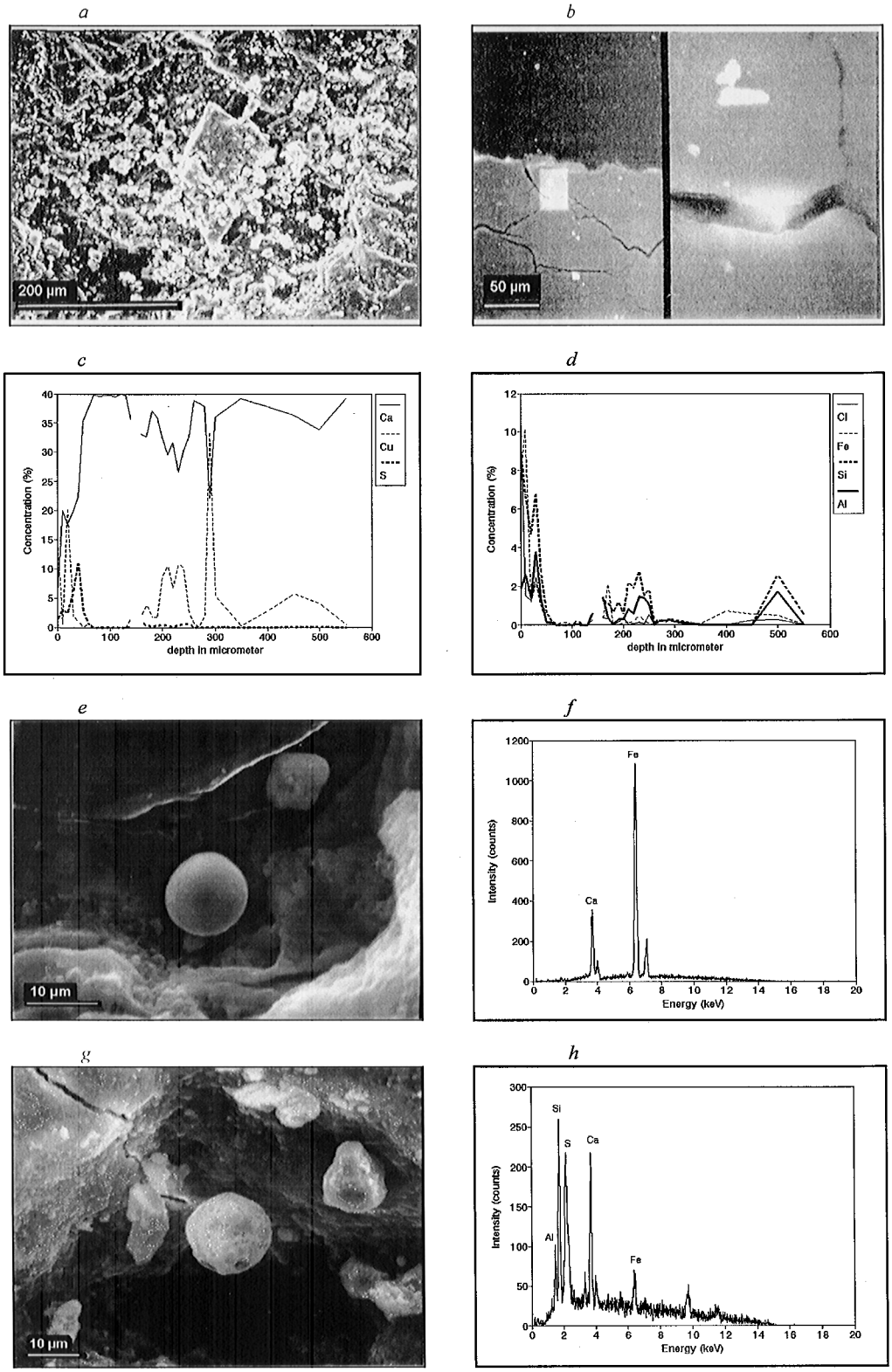

Fig. 3. Washed-out zones (sample E2: SEM micrographs (a-b-e-g); EPMA depth profiles (c-d); EDX spectra (f-h)). Intercrystalline decohesion: calcite crystals covered by quartz and recrystallized calcite with various particle formations of Cu, Fe, Si, Al, Mg, Na, Ni, K, Mn, Cr and Ti (a). Cu and Fe attain a maximum, while considerable S and Cl contents are detected (c-d). Open micro-fractures (5–6 μm) are evidenced with sub-efflorescences of gypsum (b). Fe-enriched (e-f) particles and fly ash particles, containing Al, Si, Ca and Fe, have been found (g-h).

The EPMA depth profile results and SEM-EDX micrographs and spectra enable classification of crusts and allow the formulation of hypotheses regarding growth mechanisms. On the basis of the detailed examination of the crusts several general comments can be made.

Washed-out surfaces (sample E2; Fig. 3)

Recrystallized calcite (Fig. 3a), observed at a depth of 200 μm (Fig. 3c), is more porous, as the lower Ca content indicates. It is covered by quartz and various particles containing Si, Fe, Al and Cu (Figs 3c and d). Fe-rich particles (Figs 3e and f) are observed at the interface between the recrystallized calcite and the original surface, implying that penetration occurs in depth. The latter explains the rusty-yellow colour of the washed-out marble surfaces. Fly ash particles, containing Al, Si, S, Ca and Fe, have been found (Figs 3g and h). Both particles (Figs 3e–g) can be classified as originating from coal combustion in nearby power plants (Sabbioni, 1995), because of their spherical shape and smooth surface texture.

The marble surface presents advanced inter- and intra-crystalline fracturing (Fig. 3a). Gypsum subefflorescences are observed in the open micro-fractures (Fig. 3b) from the surface and down to a depth of 300 μm (Fig. 3c), where chloride salts of K and Na also occur even down to 500 μm. It has been well known (Theoulakis and Moropoulou, 1988) that the soluble salts are subjected to outward migration due to moisture travelling through the complex pore and capillary system and finally to crystallization near the surface during the evaporation cycle. As a result, the distribution of soluble salts decreases from the surface toward the inside of the rock. Hence, the micro-fractures observed may be a consequence of crystallization pressures (Moropoulou and Theoulakis, 1991) which may cause selective fissuring, especially where different porous systems wedge like gypsum to calcite or at "necks" between macro and micropores of the same system (calcite). This mechanism could lead to detachment (granular disintegration and flaking), even up to cavitation and crater formation.

Rusty-yellow crusts (samples A1 and A2; Fig. 4)

At rusty-yellow surfaces, dissolution of calcite takes place (Fig. 4a) up to a depth of 150 μm, whereas Si, Al, Fe, Ti, K are being deposited at the surface (Fig. 4b).

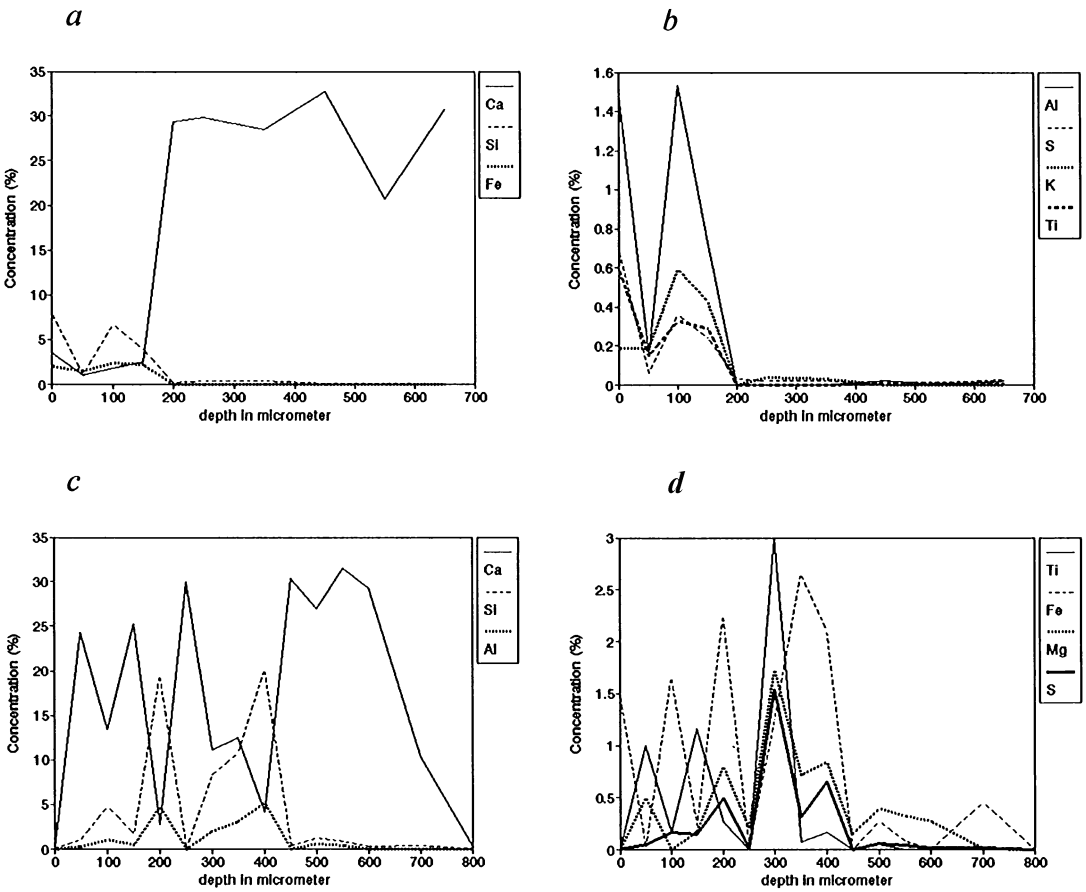

Fig. 4. Rusty-yellow crusts (sample A1: EPMA depth profiles (a-b); sample A2: EPMA depth profiles (c-d)). Dissolution of calcite (a-c) is taking place in the crust samples A1 and A2, respectively, along with the deposition of Si and Al, and impregnation with Fe and Ti (b-d).

At grey-rusty surfaces (sample A2), where water-rebound phenomena occur, an intercrystalline detachment is shown due to impregnation of the calcitic structures at a depth of 800 μm, by the alternating Ca, Si, Al peaks (Fig. 4c) followed by significant Ti, Fe, Mg and S deposits (Fig. 4d). Sample A1, the rusty-yellow crust (Fig. 4a), contains more Fe than the grey-rusty crust (Fig. 4c).

According to Skoulikidis and Papakonstantinou-Ziotis (1981), the Fe content of Pentelic marble is very low, but dissolution of calcite from the surface by rain water, CO_2 and SO_2 enables the Fe-compounds to become enriched and oxidized on the surface, giving it a golden patina. However, the Fe-content depth profile (Fig. 4a) clearly indicates Fe attack on the Pentelic marble sample A1 at the outer surface, declining almost to zero within 100–150 μm, where calcite dissolution takes place. Moreover, Fe-rich particles have been isolated and studied on the marble surfaces (Van Grieken and Torfs, 1994). The Fe-content at the crust surface is similar to the Fe-content in atmospheric particulate matter in the Eleusis area (Abazoglou *et al.*, 1990a, b), which is considerably higher than for the centre of Athens (Valaora, 1986).

Fassina *et al.* (1994) suggest that oxalate formation is responsible for the rusty-yellow patinas. However, no oxalates were identified by IR-spectrometry (Moropoulou *et al.*, 1994a, b).

Black–grey crust sections (sample E1; Fig. 5)

A matrix, rich in Ca of secondary recrystallized calcite (Fig. 5a), is shields amorphous deposit formation (Fig. 5b) rich in S-compounds and gypsum (Table 2: the SO_4^{2-}-content is 40%), whereas Si is abundant, but less than S (Fig. 5e). Quartz feldspars and Fe-oxide crystals (Fig. 5f) are also observed, along with organic particles (Figs 5g and h) enriched in S, Cl and Ca. The crust (50–180 μm in depth) is firmly attached to the open micro-fractures of the surface (50 μm). On the external surface, salt crystals are embedded in the crust (Figs 5c and d).

Gypsum formation (samples E4 and E6; Fig. 6)

Loose deposits (sample E4). The observed black and white areas (Fig. 6a) comprise gypsum (Fig. 6b) and secondary calcite, respectively. Wherever water contacts the marble surfaces, recrystallized calcite is formed. Conversely, where no such contacts are observed, loose deposits are found with gypsum, mainly comprising the black crust of 500 μm depth (Fig. 6d). A stratification of two layers is observed (Fig. 6c): in the first layer (100 μm), calcite, quartz, gypsum and feldspars are present along with spherical Fe-rich particles while in the second (400 μm), gypsum interconnected with quartz, Fe-rich spheres and Fe-oxides are mainly observed.

Grey–yellow edge of the pits formed by the cementitious encrustations (sample E6). The Si concentrations are almost the same for sample E6 (Fig. 6f) and E4 but the S and Fe concentrations are lower for sample E6 (Fig. 6g).

Surface encrustations (samples E5 and E9; Fig. 7)

Amorphous formations (sample E5, Fig. 7a) rich in Ca, Si, Al, Ti and Fe, coating secondary calcite, occur on external surfaces, while Cl (3.5%) is traced. Sample E5 is considered as cementitious crust on marble, while sample E9 is cementitious crust on limestone. The cementitious encrustations of 250–300 μm thickness (sample E5) and 2 mm (sample E9) are enriched in Ca, S, Si, Al and Fe, while, gypsum crystals (Fig. 7b) are also observed.

The Ca-content varies a lot and Si is present in the whole sample E9, on places where the Ca-concentration is lower (Figs 7c and d). High S-peaks have been observed near the surface. Si and Fe are enriched in both cementitious encrustations, S is more abundant in the crust on marble. Fly ash particles, containing Si, Ca and Fe (Figs 7e and f), originating from coal combustion, are observed.

The XRD results (Table 4) give evidence to the high calcitic content of the surface encrustations, while lower percentages of gypsum, quartz, alkali-feldspars and plagioclase, mica, chlorite and cementitious (CSH) phases are also present. As the C_vS (e.g. C_3S ($= 3CaO \cdot SiO_2$), C_2S, etc.) compounds, especially the amorphous ones, tend to react with water, changing their water content and structure, they absorb the acid rain binding SO_4^{2-}.

The FT-LMMS results of sample E9 (Figs 7g and h) show Ca and K as the most abundant cations; in the spectrum of the negative ions, mass peaks related the phosphate and sulphate, and clusters of C could be seen very clearly. No oxalate has been found in this sample.

CONCLUSIONS

For a given substrate, and specifically for white (Pentelic) marble, the influence of the heavily polluted atmosphere in the marine environment varies, resulting in several interconnected weathering patterns, mainly in the form of crusts, according to both extrinsic (microenvironment) and intrinsic (micro-structure, composition, texture) factors.

The various material–environment interactions taking place are characterized by:

- rusty-yellow patinas on washed-out areas,
- firmly attached black–grey crusts where the marble surface is in contact with water,
- black loose deposits and gypsum in rain-water-sheltered areas and
- cementitious crusts coating and pitting horizontal surfaces.

Analyses of dust and deposits give indications of the origin of the various crust formations. In particular,

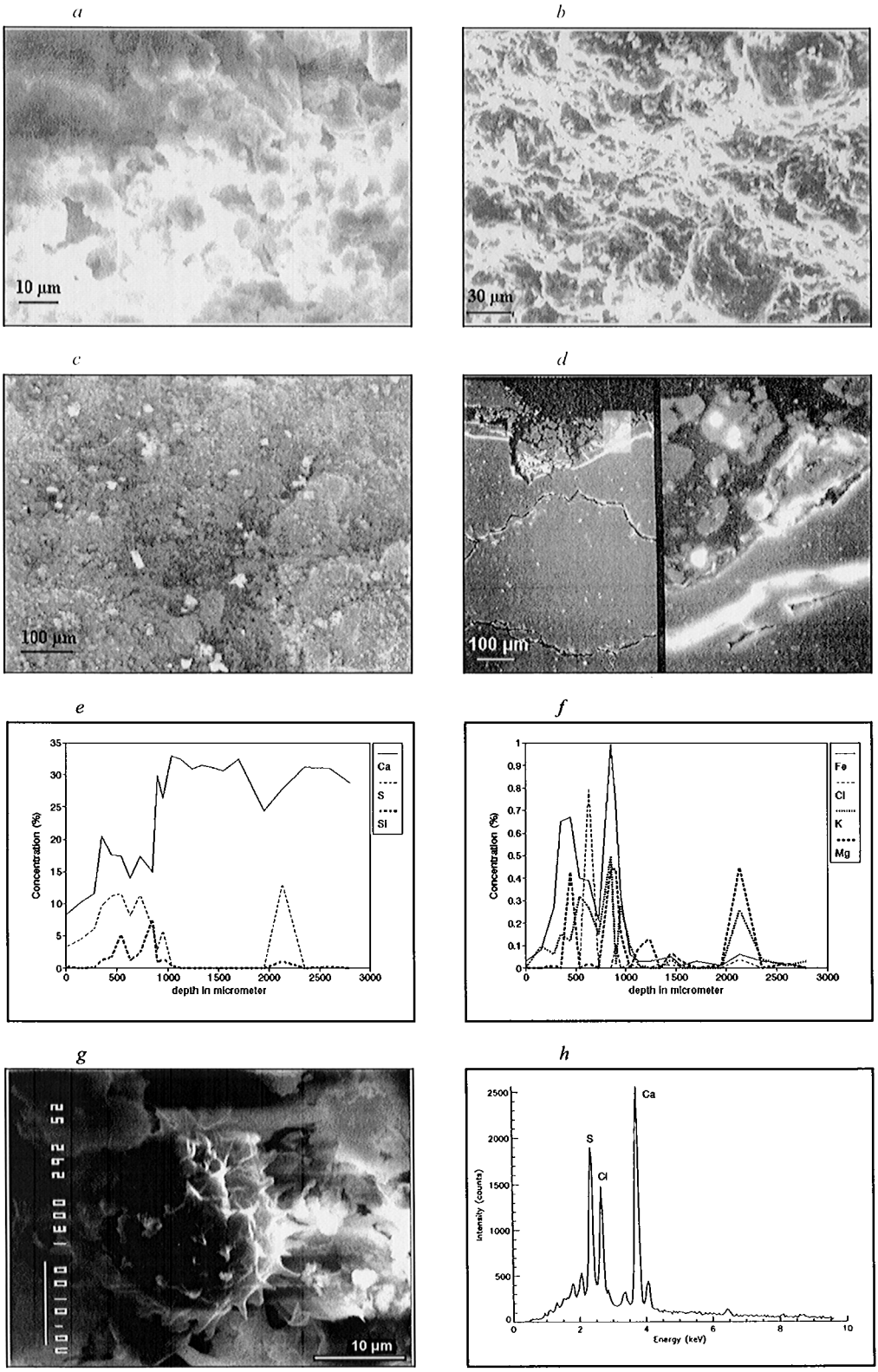

Fig. 5. Black–grey crust (sample E1: SEM micrographs (a-b-c-d-g); EPMA depth profiles (e-f); EDX spectrum (h)). A calcitic microcrystalline matrix (a) shields carbonaceous particles (b-d) and amorphous deposits (b) rich in S (e). Significant percentages of Si, Fe, Cl, K and Mg are also evidenced (f). Salt crystals are observed on the external surfaces (c). The crust of 50–180 μm (d) is firmly attached to the open micro-fractures of the surface (50 μm), showing carbonaceous particles (g-h) with Ca, S, Cl compounds (h).

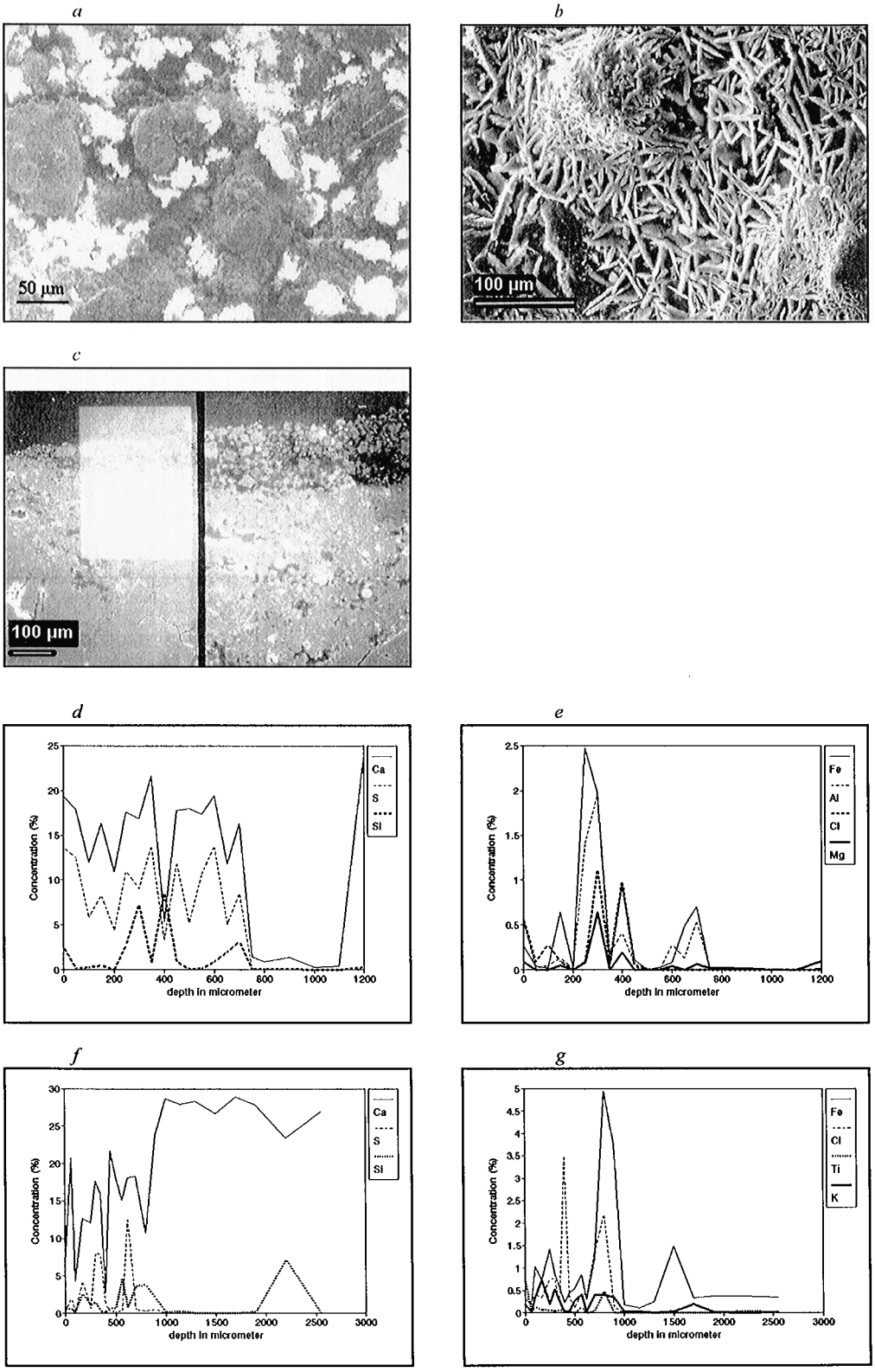

Fig. 6. Gypsum formation (sample E4: SEM micrographs (a-b-c); EPMA depth profiles (d-e); sample E6: EPMA depth profiles (f-g)). Loose deposits (sample E4) (a): secondary calcite is observed at white areas in contact with water and crystals of gypsum at the (water sheltered) dark ones (b). Stratification of the crust in two layers (100 and 400 μm) (c) is evidenced by the different porosity. Grey–yellow crust (sample E6) at the edge of the pit formed by the cementitious encrustation: gypsum crystals are formed on a swallow pit of main elements—Ca, S, Si, Fe—show more or less the same evolution, for the samples E4, E6 respectively, the Cl being more important at sample E6.

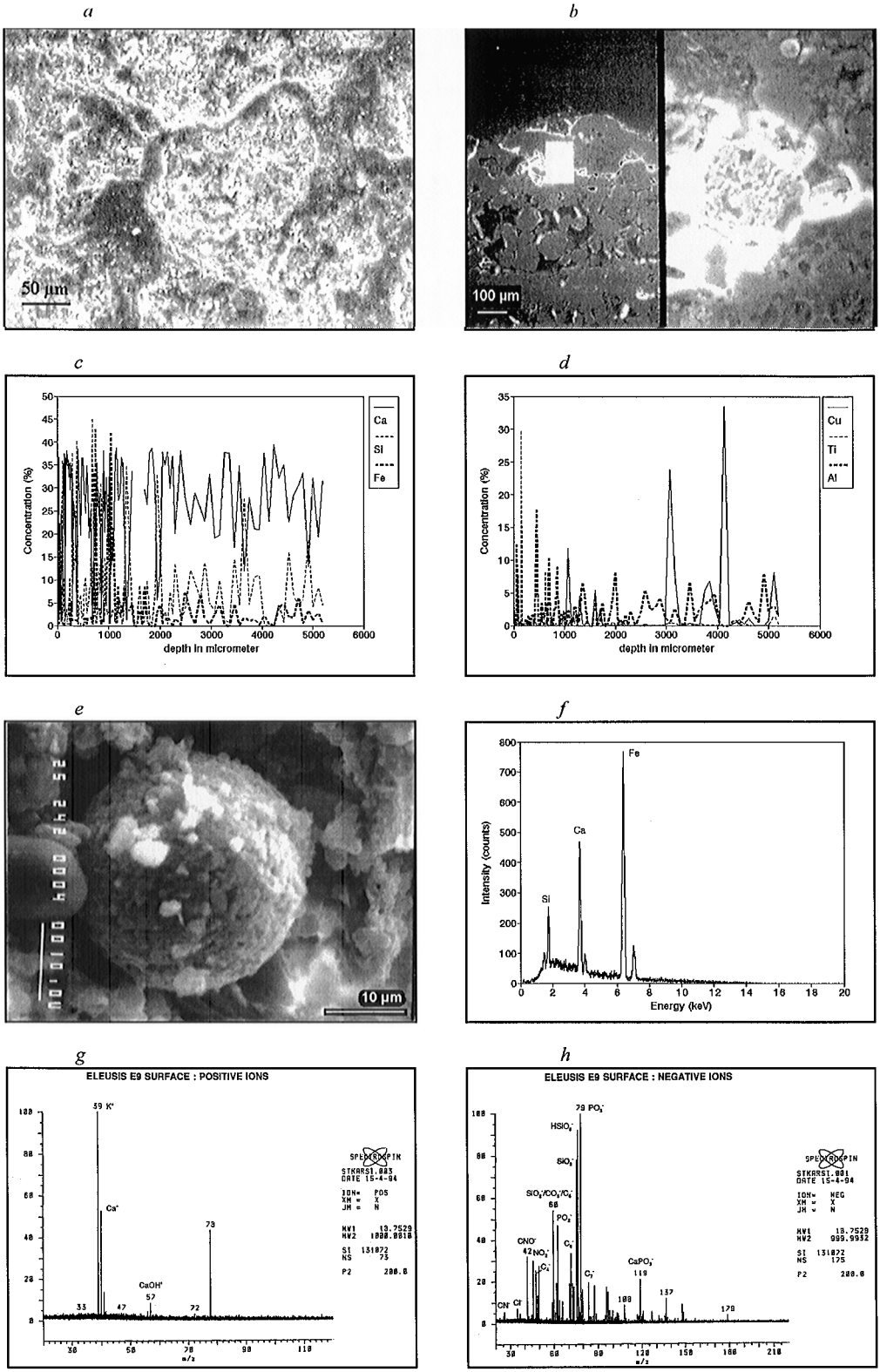

Fig. 7. Cementitious encrustations (sample E5: SEM micrographs (a-b); sample E9: EPMA depth profiles (c-d); SEM micrograph (e); EDX spectrum (f); FT-LMMS results (g-h)). Amorphous and cementitious formations (a) rich in alkalisilicate (Ca-Si) compounds, Fe, Cu, Ti and Al (c-d), are coating the marble surface. The cementitious encrustations vary in depth from 250 to 300 μm (sample E5: b) to 2 mm (sample E9) and present also gypsum crystals in the intercrystalline voids. Fly ash particles rich in Fe, Ca, Si (e-f) show the role of the cement industry emissions. The FT-LMMS spectra indicate the presence of portlandite (g) along with alkalisilicate hydra tes (h) (sample E9).

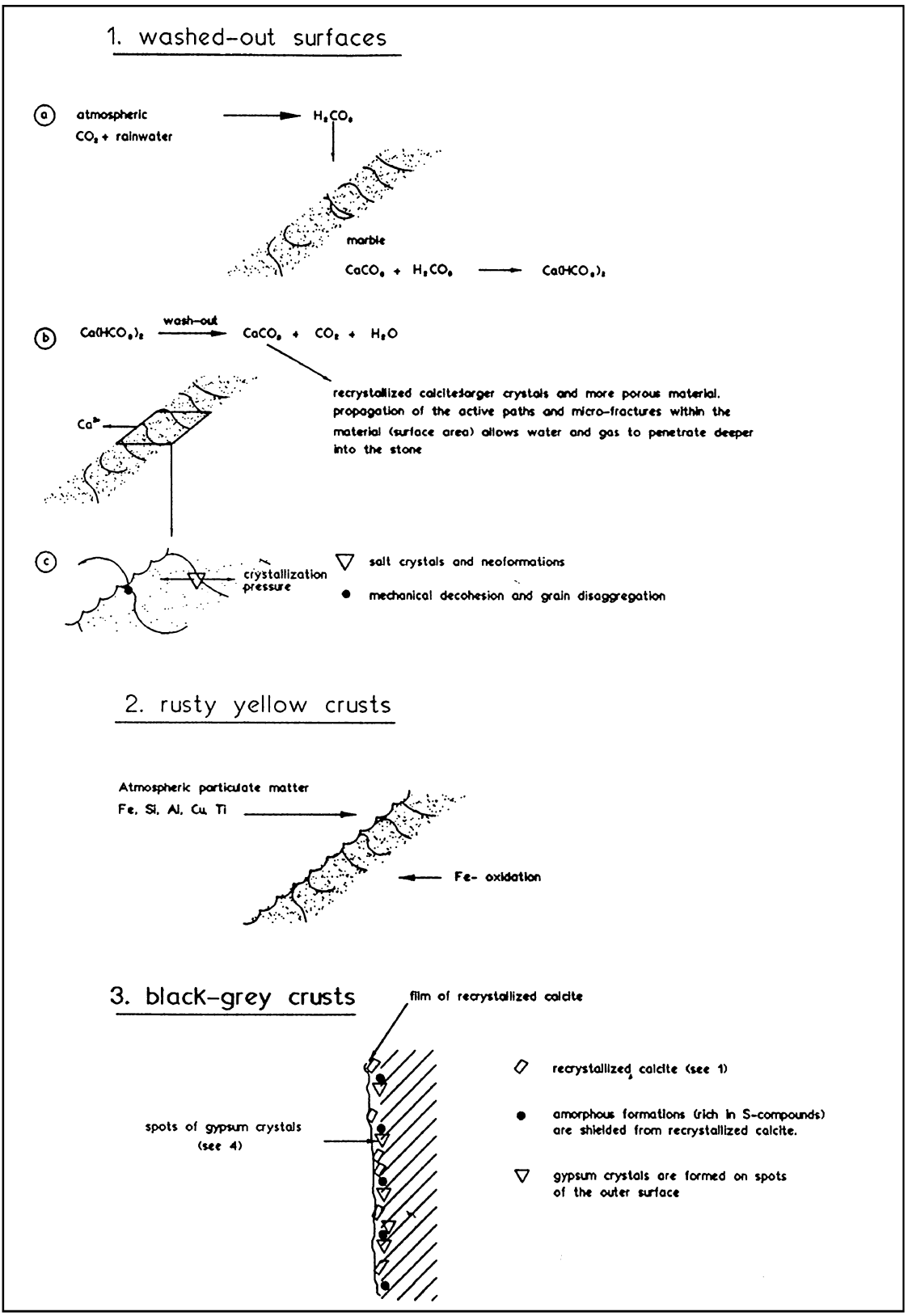

Fig. 8 (continued opposite). Schematic representation of the processes involved during the creation of the crusts.

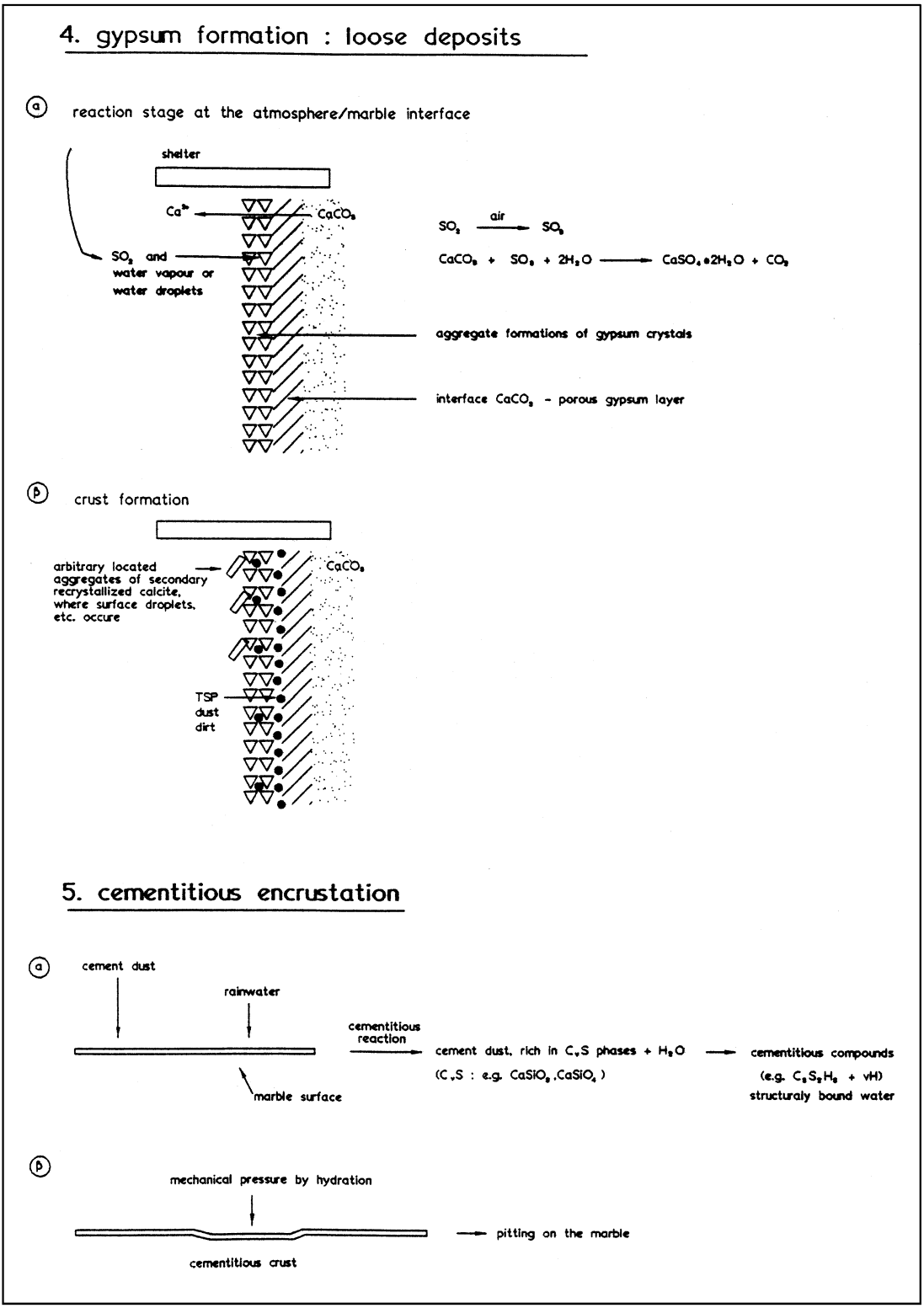

Fig. 8. *Continued* (caption on previous page).

cement industry deposits could be related to the surface encrustations, particles rich in Fe to the rusty-yellow patinas of the washed-out surfaces, the high S-content of suspended particles and high SO_2 concentrations lead to the gypsum formation, black loose deposits and the black-grey crusts, where recrystallized calcite shields amorphous deposit impurities rich in S and Si compounds.

Embedded salt crystals indicate a marine source for some of the salts contributing to damage of the stone surface. The processes that take place during the creation of the crusts are represented in the schemes, shown in Fig. 8. Thus, the alteration of the microporosity is confirmed as well as the alteration in the chemical composition.

Acknowledgements—This work was partially supported by the European Union under contract EV5V-CT92-0102 and the coordination of CUM–Prof. F. Zezza. We are grateful to Mr. P. Papapetrou, Mayor of Eleusis and to Mr. A. Christidis, Director of SELER (Station of Pollution Control in Eleusis), for their valuable collaboration. Acknowledgements are made to the 3rd Ephoriate of Classical Antiquities, as well as to the Archaeological Society, for their permission to work at the historical site of the Sanctuary of Demeter in Eleusis.

REFERENCES

Abazoglou, G., Christidis, A. and Mourikis, D. (1990a) The dust fall at the Thriasian plain. *Panhellenic Society of Chemical Engineers* **87**, 10–23.

Abazoglou, G., Christidis, A. and Mourikis, D. (1990b) The dust fall at the Thriasian plain. *Panhellenic Society of Chemical Engineers* **88**, 18–25.

Camuffo, D., Del Monte, M., Sabbioni, C. and Vittori, O. (1982) Wetting, deterioration and visual features of stone surfaces in an urban area. *Atmospheric Environment* **16**, 2253–2259.

Camuffo, D., Del Monte, M. and Sabbioni, C. (1983) Origin and growth mechanisms of the sulphated crusts on urban limestone. *Water Air Soil Pollution* **19**, 351–359.

Camuffo, D., Del Monte, M. and Sabbioni, C. (1987) Influenza delle precipitazioni e della condensazione sul degrado superficiale dei monumenti in marmo e calcare. *Materiali Lapidei* (Bollettino d' Arte del Ministero per i Beni Culturali e Ambientali) **41**, 15–36.

Del Monte, M., Sabbioni, C., Ventura, A. and Zappia, G. (1984) Crystal growth from carbonaceous particles. *Science of Total Environment* **36**, 247–254.

Dickinson, C., Haneef, S., Johnson, J. B., Thompson, G. E. and Wood, G. C. (1988) Effects of air pollution on historic buildings and monuments and the scientific basis for conservation. *Progress Report*. EC contract EV4V.0053.UK(H), UMIST, Manchester.

Fassina, V., Rossetti, M., Oddone, M., Mazzochini, S. and Calogero, S. (1994) Marine spray and polluted atmosphere as factors of damage to monuments in the Mediterranean coastal environment. An analytical study of some samples from the Sanctuary of Demeter in Eleusis (Athens). In *Proceedings of the 3rd International Symposium on the Conservation of Monuments in the Mediterranean Basin*, eds. V. Fassina, H. Ott and F. Zezza, pp. 287–294. Soprintendenza ai Beni Artistici e Storici di Venezia.

Moropoulou, A. and Theoulakis, P. (1991) Favourable conditions to destructive NaCl crystallization into the porous sandstone of the medieval city of Rhodes. In *Proceedings of the 2nd International Symposium on the Conservation of Monuments in the Mediterranean Basin*, eds D. Decrouez, J. Chamay, and F. Zezza, pp. 493–499. Ville de Genève - Museum d'Histoire naturelle and Musée d'Art et d'Histoire.

Moropoulou, A., Zezza, F., Aires Barros, L., Christaras, B., Fassina, V., Fitzner, B., Fournaraki-Kassoli, A., Galan, E. and Van Grieken, R. (1994a) Marine spray and polluted atmosphere as factors of damage to monument in the Mediterranean coastal environment—a preliminary approach to the case of Demeter Sanctuary in Eleusis. In *Proceedings of the 3rd International Symposium on the Conservation of Monuments in the Mediterranean Basin*, eds V. Fassina, H. Ott and F. Zezza, pp. 275–286. Soprintendenza ai Beni Artistici e Storici di Venezia.

Moropoulou, A., Bisbikou, K. and Koui, M. (1994b) Marine spray and polluted atmosphere as factors of damage to monument in the Mediterranean coastal environment. *Semestrial Report No 3. R and D Programme in the Field of Environment*. Co-ord. Zezza F., EU Contract No EV5V-CT92-0102.

Moropoulou, A. and Bisbikou, K. (1995) Environmental monitoring and damage assessment at the ancient Sanctuary of Eleusis, Greece. In *Proceedings of the Symposium Materials Issues in Art and Archaeology*, eds. J. R. Druzik and P. B. Vandiver, vol. **352**, pp. 745–757. Materials Research Society.

Moropoulou, A., Bisbikou, K., Christaras, B., Kassoli-Fournaraki, A., Zouros, N., Makedon, Th., Fitzner, B. and Heinrichs, K. (1995) Examination of the weathering susceptibility of the building stones of Demeter Sanctuary in Eleusis: 1. Origin, petrography and physical, mechanical and microstructural properties. *Bollettino Geofisico* **18**, 37–48.

Preka-Alexandri, K. (1991) *Eleusis*. Ed. Kypraiou E., Ministry of Culture, Archaeological Receipts Fund, M.A. Moatsos Graphic Arts, Athens.

Rodriguez-Navarro, C. and Sebastian, E. (1995) Role of particulate matter from vehicle exhaust on porous building stones (limestone) sulfation. *Science of Total Environment* **187**, 79–91.

Sabbioni, C. (1995) Contribution of atmospheric deposition to the formation of damage layers. *Science of Total Environment* **167**, 49–55.

Skoulikidis, Th. and Charalambous, D. (1981) Mechanism of sulphation by atmospheric SO_2 of the limestones and marbles of the ancient monuments and statues, II. Hypothesis concerning the rate determining step in the process of sulphation, and its experimental confirmation, *British Corrosion Journal* **16**, 70–76.

Skoulikidis, Th. and Papakonstantinou-Ziotis, E. (1981) Mechanism of sulphation by atmospheric SO_2 of the limestones and marbles of the ancient monuments and statues, I. Observations *in situ* (Acropolis) and laboratory measurements. *British Corrosion Journal* **16**, 63–69.

Theoulakis, P. and Moropoulou, A. (1988) Mechanism of deterioration of the sandstone of the Medieval City and the Castle of Rhodes. In *Proceedings of the 6th International Congress on Deterioration and Conservation of Stone*, ed. J. Ciabach, pp. 86–96. Nicholas Copernicus University, Torun, Poland.

Valaora, G. (1986) Air pollution in Athens, Greece. *The Environmental Professional* **8**, 149–164.

Van Espen, P., Janssens, K. and Nobels, J. (1986) AXIL-PC, software for the analysis of complex X-ray spectra. *Chemometrics. Intelligent Laboratory System* **1**, 109–114.

Van Grieken, R. and Torfs, K. (1994) Marine spray and polluted atmosphere as factors of damage to monument in the Mediterranean coastal environment. *Semestrial Report No* 3. *R and D Programme in the Field of Environment*. Co-ord. Zezza F., EU Contract No EV5V-CT92-0102.

Van Vaeck, L., Van Roy, W., Struyf, H., Adams, F. and Caravatti, P. (1993) Development of a laser microprobe Fourier transform mass spectrometer with external ion source. *Rapid Communications in Mass Spectrometry* **7**, 323–331.

Zezza, F. (1994) Marine spray and polluted atmosphere as factors of damage to monuments in the Mediterranean coastal environment. In *Proceedings of the 3rd International Symposium on the Conservation of Monuments in the Mediterranean Basin*, eds V. Fassina, H. Ott and F. Zezza, pp. 269–274. Soprintendenza ai Beni Artistici e Storici di Venezia.